High-order simulation of hypersonic nonequilibrium flows on overset grids

By A. Lani, B. Sjögreen AND H. C. Yee

1. Motivation and objectives

The time-accurate unsteady 3D compressible flow solver ADPDIS3D is supported by a grant from the Department of Energy (DOE) SciDAC program through the Science Application Partnership (SAP) initiative. The objective of this grant is to develop, implement and validate this variable high-order 3-D multiblock overlapping (overset) grid solver for turbulence with strong shocks and density variations. ADPDIS3D includes capabilities for both direct numerical simulation (DNS), resolving all scales of the flow fields, and large eddy simulation (LES) modeling the small turbulent scales. One of the unique features of the code is the ability to perform DNS and LES computations in non-trivial geometries through the use of overset curvilinear grids. ADPDIS3D contains a large number of high-order numerical schemes and shock-capturing numerical schemes for accurate unsteady computations for flow speeds that range from nearly incompressible to hypersonic speeds. Importantly, ADPDIS3D implements many innovative low dissipative algorithms that adaptively use numerical dissipation from shock-capturing schemes as post-processing filters on non-dissipative high-order centered schemes. These schemes were especially designed for improved accuracy over standard high-order shock-capturing schemes in capturing of turbulence with strong shocks and density variations. For a description of algorithms and their performances, including a detailed LES computation of temporal-evolving mixing layer, see e.g., Sjögreen & Yee (2009), Yee & Sjögreen (2006), Yee *et al.* (2008), Yee & Sjögreen (2009), Yee *et al.* (2010), Wang *et al.* (2010), Hadjadj *et al.* (2010). Furthermore, ADPDIS3D contains solvers for standard compressible flow, compressible non-ideal MHD, and chemical nonequilibrium hypersonic flows. For a more detailed description see Sjögreen *et al.* (2009).

Multiscale turbulence with strong shocks and flows containing both steady and unsteady components requires mixing of numerical methods and switching on the appropriate scheme in the appropriate subdomains of the flow fields, even under the multiblock grid or adaptive grid refinement framework. It is a non-trivial task to find adaptive schemes that both correctly identify different flow features, and perform switching locally to a suitable method without seriously affecting the overall accuracy of the method. While low dissipative sixth- or higher-order shock-capturing filter methods are appropriate for unsteady turbulence with shocklets, third-order or lower shock-capturing methods are more effective for strong steady or nearly steady shocks in terms of convergence. An important application for the subject flow physics is chemical and thermo-chemical nonequilibrium hypersonic turbulence flows. In order to minimize the shortcomings of low-order and high-order shock-capturing schemes for the subject flows, ADPDIS3D contains overset grids with different types of spatial schemes and orders of accuracy on the chosen block grids as an efficient method in combating the difficulty. It is anticipated that this particular overset grid framework capability with highly modular design will allow an optimum synthesis of these new algorithms in such a way that the most appropriate spa-

tial discretizations can be tailored for each particular region of the flow. In addition, for nonequilibrium/combustion flows, ADPDIS3D has been merged with the MUTATION library (version 1.3, Thierry Magin, private communication) for more accurate transport, chemical/thermo properties.

The overset grid implementation for a perfect gas has been validated in Sjögreen & Yee (2009) and Yee & Sjögreen (2006). With additional improvements (Wang *et al.* 2010), the same numerical methods and the same overset grid framework for perfect gas can be carried over to chemical and certain thermo-chemical nonequilibrium flows. This is a work-in-progress report of the first step of a multistep validation process for the nonequilibrium implementation. Only 2-D five-species one-temperature blunt body inviscid and viscous flows are considered for the present validation. In the considered test case, the flow consists of a major steady bow shock and smooth flow on the rest of the computational region. Unlike the standard pseudo time-marching to the steady state, in order to asses the capability of unsteady computations, the computations are time accurate. In addition, due to the steady flow nature of the test case, high-order filter schemes that were not designed for efficient convergence to the steady states will not be considered. Only a second-order TVD scheme and fifth-, seventh- and ninth-order WENO (WENO5, WENO7 and WENO9) using the Lax-Friedrichs flux schemes are considered.

2. Flow Solver

2.1. *Governing equations*

The system of governing equations for a gas mixture in thermodynamic equilibrium and chemical nonequilibrium can be expressed in conservative form as

$$\mathbf{U}_t + (\mathbf{F_k}(\mathbf{U}))_{x_k} + (\mathbf{G_k}(\mathbf{U}))_{x_k} = \mathbf{S}(\mathbf{U}), \quad k = 1, .., 3, \tag{2.1}$$

where $\mathbf{U} = (\rho_s, \ \rho\mathbf{v}, \ \rho E)^T$ are the conservative variables, ρ_s the partial densities, with $s = 1, \ldots, N_s$ for a mixture of N_s species. The convective and diffusive fluxes, $\mathbf{F_k}$ and $\mathbf{G_k}$, are, respectively, given by

$$\mathbf{F_k} = \begin{pmatrix} \rho_s v_k \\ \rho v_k v_l + p\delta_{kl} \\ \rho v_k H \end{pmatrix}, \quad \mathbf{G_k} = \begin{pmatrix} \rho_s v_{sk} \\ -\tau_{kl} \\ -\tau_{kl} v_l + q_k + \sum_s \rho_s v_{sk} h_s \end{pmatrix}, \quad l = 1, .., 3. \tag{2.2}$$

The mixture total density, the pressure and the total energy per unit volume appearing in (2.2) are computed with

$$\rho = \sum_s \rho_s, \quad p = RT \sum_{s=1}^{N_s} \frac{\rho_s}{M_s}, \quad \rho E = \sum_{s=1}^{N_s} \rho_s \left(e_s(T) + h_s^0\right) + \frac{1}{2}\rho v^2, \tag{2.3}$$

where h_s^0 are the species formation enthalpies. The exact expressions for the species internal energies $e_s(T)$, including roto-translational, vibrational and electronic contributions, can be found in Abeele (2000). The viscous stresses τ_{kl} and the conduction heat fluxes q_k can be expressed as follows:

$$\tau_{kl} = \mu \left[\left(\frac{\partial u_l}{\partial x_k} + \frac{\partial u_k}{\partial x_l} \right) - \frac{2}{3} \nabla \cdot \mathbf{v} \delta_{kl} \right], \quad q_k = -(\lambda^t + \lambda^r)\frac{\partial T}{\partial x_k}. \tag{2.4}$$

Here, the computation of transport coefficients and fluxes is based on the modified Chapman-Enskog perturbative analysis for partially ionized plasmas and on efficient iterative algorithms (Magin & Degrez 2004) for solving the linear systems from which shear viscosity μ and translational thermal conductivity λ^t can be obtained. The rotational thermal conductivity λ^r is calculated with the Eucken approximation (Abeele 2000). The diffusion fluxes $\rho_s v_{sk}$ are computed by solving the Stefan-Maxwell system (Abeele 2000), i.e., a linear system in the diffusion fluxes consisting of as many equations as those of the mixture chemical species, supplemented by the auxiliary condition of zero sum for the diffusion fluxes. The source term in (2.1) reads

$$\mathbf{S} = \begin{pmatrix} \dot{\omega}_s \\ 0 \\ 0 \end{pmatrix}, \quad \dot{\omega}_s = M_s \sum_{r=1}^{Nr} \left(\nu_{sr}^{''} - \nu_{sr}^{'} \right) \left\{ k_{fr} \prod_{m=1}^{Ns} \left(\frac{\rho_m}{M_m} \right)^{\nu_{mr}^{'}} - k_{br} \prod_{m=1}^{Ns} \left(\frac{\rho_m}{M_m} \right)^{\nu_{mr}^{''}} \right\},$$

(2.5)

with $\dot{\omega}_s$ expressing the mass production/destruction term for chemical species s. In Eq. 2.5, the forward reaction rates coefficients $k_{fr} = A_{f,r} T^{n_{f,r}} \exp(-E_{f,r}/kT)$ are expressed by means of Arrhenius' law. The backward reactions rates coefficients are computed as $k_{b,r} = k_{f,r}/K_{c,r}^{eq}$, where $K_{c,r}^{eq}$ is the equilibrium constant. In the present work, all thermodynamic, transport, chemical properties have been calculated by the MUTATION library (version 1.3, Thierry Magin) which provides state-of-the-art models described extensively in Abeele (2000) and Magin & Degrez (2004), to whom any interested reader is referred.

2.2. *Numerical Discretization*

In spite of the vast number of low-dissipative high-order schemes contained in ADPDIS3D (Sjögreen & Yee 2009; Yee & Sjögreen 2006; Yee *et al.* 2008; Yee & Sjögreen 2009; Yee *et al.* 2010; Hadjadj *et al.* 2010; Wang *et al.* 2010), in the present preliminary study, only the second-order Harten-Yee TVD (see Yee (1989) and references cited therein for details) and WENO Lax-Friedrichs schemes are considered for the discretization of the inviscid flux derivative. A matching order of discretization as the inviscid flux derivatives is applied to the viscous flux derivatives. A pointwise evaluation is used for the reacting term. Explicit second-order Runge-Kutta (RK2) is used in a time-accurate mode for the time discretization. Due to the explicit time-accurate computation, a very large number of iterations should be expected. With a sufficiently fine grid, unsteady features of the flow field, if they exit, can be observed with this time-accurate approach.

2.2.1. *Finite difference WENO schemes*

Consider a scalar hyperbolic conservation law with source term in one dimension:

$$u_t + f(u)_x = s(u),$$

(2.6)

with a positive advection speed $f'(u) \geq 0$. For a finite difference discretization, evolve the point values u_i at mesh points x_i in time with a uniform mesh size Δx for simplicity. The spatial derivative in Eq. 2.6 is approximated by a conservative flux difference:

$$f(u)_x|_{x=x_i} \approx \frac{1}{\Delta x} \left(\tilde{f}_{i+\frac{1}{2}} - \tilde{f}_{i-\frac{1}{2}} \right).$$

(2.7)

The numerical flux $\tilde{f}_{i+\frac{1}{2}}$ is computed through the neighboring point values $f_j = f(u_j)$. For a $(2k-1)$-th order WENO scheme, first k numerical fluxes are computed by

$$\tilde{f}^{(r)}_{i+\frac{1}{2}} = \sum_{j=0}^{k-1} c_{rj} f(x_{i-r+j}), \quad r = 0, \ldots, k-1, \tag{2.8}$$

corresponding to k different candidate stencils $S_r(i) = x_{i-r}, \ldots, x_{i-r+k-1}$. Each of these k numerical fluxes is $k-th$-order accurate. For example, when $k = 3$ (fifth-order WENO), the three third-order accurate numerical fluxes are given by

$$\tilde{f}^{(0)}_{i+\frac{1}{2}} = \frac{1}{3} f_i + \frac{5}{6} f_{i+1} - \frac{1}{6} f_{i+2} \tag{2.9}$$

$$\tilde{f}^{(1)}_{i+\frac{1}{2}} = -\frac{1}{6} f_{i-1} + \frac{5}{6} f_i + \frac{1}{3} f_{i+1} \tag{2.10}$$

$$\tilde{f}^{(2)}_{i+\frac{1}{2}} = \frac{1}{3} f_{i-2} - \frac{7}{6} f_{i-1} + \frac{11}{6} f_i. \tag{2.11}$$

The $(2k-1)$-th order WENO flux consists of a convex combination of all these k fluxes:

$$\tilde{f}_{i+\frac{1}{2}} = \sum_{r=0}^{k-1} w_r \tilde{f}^{(r)}_{i+\frac{1}{2}}. \tag{2.12}$$

Here, the conditions $w_r \geq 0$ and $\sum_{r=0}^{k-1} w_r = 1$ hold for the nonlinear weights which are defined as

$$w_r = \frac{\alpha_r}{\sum_{s=0}^{k-1} \alpha_s}, \quad \alpha_r = \frac{d_r}{(\epsilon + \beta_r)^2}, \tag{2.13}$$

where the linear weights d_r yield the required $(2k-1)$-th order accuracy, β_r are the so-called *smoothness indicators* which measure the smoothness of the function $f(u(x))$ within the stencil $S_r(i)$. ϵ is a constant which prevents the denominator from becoming zero (typically assumed to be 10^{-6}). An example of linear weights and smoothness indicators for $k = 3$ can be found in Yee *et al.* (2008). The procedure for the case with $f'(u) \leq 0$ is mirror symmetric with respect to $i + \frac{1}{2}$. An upwinding mechanism, necessary for stabilizing the scheme, can be embodied in the WENO schemes by a global flux splitting, such as Roe with entropy fix (WENO-RF) or Lax-Friedrichs, as described in Jiang & Shu (1996). The latter, in particular, is defined as

$$f^{\pm}(u, x) = \frac{1}{2}(f(u, x) \pm \lambda \alpha u), \quad \alpha = \mathtt{max}_u |f'(u)|, \quad \lambda = 1. \tag{2.14}$$

The WENO procedure is applied to both f^+ and f^- with upwind biased stencils. The scheme for which the `max` is taken globally along the line of computation is commonly denoted WENO-LF. A well-balanced version (WENO-LF-WB) of the baseline WENO-LF, capable of preserving certain non-trivial steady-state solutions exactly and resolving accurately relatively small perturbations around the steady solution up to machine accuracy is introduced in Wang *et al.* (2009). In one form of WENO-LF-WB, in order not to affect stability near shocks, λ is no longer constant but acts as an equilibrium limiter:

$$\lambda := \mathtt{max}(\mathtt{min}(1, \chi_1), \ldots, \mathtt{min}(1, \chi_m)), \quad \chi_j = \frac{(|r_j^+| + |r_j^-|)^2}{|r_j^+|^2 + |r_j^-|^2 + \epsilon}, \tag{2.15}$$

with $r_j^{\pm} = r_j(u_{i\pm1}, x_i) - r_j(u_i, x_i)$ being differences of some known functions (e.g., computed pressure or density) which should be close to zero near the specific steady state. ϵ is

again a small quantity (10^{-6}) to avoid division by zero. Both baseline WENO-LF (fifth-, seventh-, ninth-order) and WENO-LF-WB (fifth- and seventh-order) schemes have been employed for our numerical experiments. More details can be found in Jiang & Shu (1996), Wang *et al.* (2009) and Wang *et al.* (2010).

2.2.2. *Finite difference Harten-Yee TVD*

For the x inviscid flux derivatives $\mathbf{F}$, the numerical flux by the second-order Harten-Yee TVD scheme can be written (with all the y and z indices suppressed) as

$$\tilde{\mathbf{F}}_{j+\frac{1}{2}} = \frac{1}{2}\left(\mathbf{F}_j + \mathbf{F}_{j+1} + \mathbf{R}_{j+\frac{1}{2}}\boldsymbol{\Phi}_{j+\frac{1}{2}}\right), \tag{2.16}$$

where $\mathbf{R}$ is the matrix of right eigenvectors for the convective flux Jacobian and each component of $\boldsymbol{\Phi}_{j+\frac{1}{2}}$ denoted by $\phi^l_{j+\frac{1}{2}}$ with $l = N_s + 4$ is given by

$$\phi^l_{j+\frac{1}{2}} = \frac{1}{2}\psi\left(a^l_{j+\frac{1}{2}}\right)\left(g^l_j + g^l_{j+1}\right) - \psi\left(a^l_{j+\frac{1}{2}} + \gamma^l_{j+\frac{1}{2}}\right)\alpha^l_{j+\frac{1}{2}}, \tag{2.17}$$

with $\alpha^l_{j+\frac{1}{2}}$ being elements of $\mathbf{R}^{-1}_{j+\frac{1}{2}}(\mathbf{U}_{j+1} - \mathbf{U}_j)$ and

$$\gamma^l_{j+\frac{1}{2}} = \frac{1}{2}\psi\left(a^l_{j+\frac{1}{2}}\right)\begin{cases} (g^l_{j+1} - g^l_j)/\alpha^l_{j+\frac{1}{2}} & \alpha^l_{j+\frac{1}{2}} \neq 0 \\ 0 & \alpha^l_{j+\frac{1}{2}} = 0 \end{cases}, \tag{2.18}$$

where ψ is the entropy correction function defined in Harten (1984). In all the following computations, the most diffusive limiter, namely $g^l_j = \mathtt{minmod}\left(\alpha^l_{j-\frac{1}{2}}, \alpha^l_{j+\frac{1}{2}}\right)$, has been used just for validation purposes, because of its fast convergence properties to steady state. Accuracy comparison among schemes must take this fact into consideration.

3. Results

For our inviscid and viscous numerical experiments, a 2D test case simulating high-speed air flow around a $1[m]$ radius cylinder was chosen. The corresponding free-stream and wall conditions (for the viscous case) are given in Table 1. This test case was computed by Peter Gnoffo (private communication) and further studied by Dr. Xiaowen Wang from the UCLA SciDAC team. In this section, his numerical analysis is referred to as *Wang's study* (not to be confused with the Wei Wang et al.'s well-balanced schemes for nonequilibrium flows). The physico-chemical model used in the present work does not consider thermal nonequilibrium as in Wang's study, but uses more sophisticated and computationally expensive thermodynamic and transport properties (see Section 2.1 for details) as opposed to energy-fitting polynomials and mixture rules. The chemical reaction rate coefficients for characterizing the neutral air mixture are taken from Park (1993) by neglecting reactions involving ions and electrons. In the following section the performance of TVD and WENO schemes (fifth-, seventh- and ninth-order) on the inviscid case on single-block and overset meshes is analyzed at first. Secondly, some results on the viscous case, again on single-block and overset meshes, are shown, but only for the TVD scheme (simulation with WENO is still work in progress). A grid convergence study has only been performed for the single-block case for simplicity. Since the simulations have been run in unsteady mode, the residual tracking has not been used as a convergence criterion, but computations have been run for long enough (typically up to

M_∞	$\rho_\infty[kg/m^3]$	$U_\infty[m/s]$	$T_\infty[K]$	$T_w[K]$	Re_∞
17.64	0.0001	5000	200	553.3	37634.8

TABLE 1. Free-stream and wall conditions for Gnoffo's test case.

500,000 iterations and 2,000,000 iterations for inviscid and viscous cases, respectively, using a CFL number up to 0.5) to let the flow fully establish.

3.1. *Inviscid flow: TVD versus WENO on single-block mesh*

This case has been run on two meshes: coarse (61 x 129 nodes) and fine (4 times finer in both directions). In Figures 1 and 2 TVD and WENO-LF solutions are compared on the coarse mesh in terms of pressure and temperature profiles on the stagnation line. Here, WENO schemes and TVD show a negligible difference on the shock standoff distance and on the peak temperature (about 1%). WENO predicts a slightly sharper profile. Grid convergence is achieved on the fine mesh, since all differences between TVD and WENO completely disappear, as testified by the pressure and temperature profiles in Figures 3 and 4, where all schemes are compared. This appears even clearer in Figure 5, where only TVD and WENO5-LF are compared on the two meshes in terms of temperature. The shock gets sharper and steeper, especially for TVD and the peak temperature increases about 6% for both schemes, as highlighted by Figure 6. On both coarse and fine meshes, WENO5 and WENO7 deliver a clean oscillation-free solution, whereas the WENO9-LF scheme gives severe spurious oscillations on all flow quantities (except for the x-velocity component), particularly on the pressure, as shown in Figures 1 and 3. This oscillating behavior tends to amplify towards the wall and, as the mesh gets finer, tends to increase in wave number and decrease in amplitude. This phenomenon was not identified in Wang *et al.* (2009) or Wang *et al.* (2010), where at most WENO5 was used and only on 1D cases with shock. Another well-known example of a problem driven by multidimensionality in high-speed flows is the carbuncle, which does not appear in our case, because the TVD scheme includes a suitable multidimensional entropy fix (Yee 1989).

3.2. *Inviscid flow: TVD versus WENO on overset mesh*

The overset grid used for this case has three-blocks, namely background (123x122 nodes), shock (201x40 nodes), body (123x40 nodes) and its upper half is shown in Figure 7. The flow solution in terms of Mach number contours is shown in Figure 8. Here, solutions yield by TVD, WENO5-LF and WENO7-LF are superposed, but they are barely distinguishable one from the other. In particular, a smooth solution transition from one block to another can be noticed, even in the post-shock region where all three mesh blocks overlap. Figure 9 indicates a temperature stagnation line profile comparison. As in the coarse single-block grid case, the standoff distances between TVD and WENO are slightly different and WENO predicts a 2% higher temperature peak. The overall quality of the solution on the overset mesh is comparable to that on the fine single-block mesh. Finally, temperature stagnation profiles computed by WENO5-LF, WENO7-LF, WENO5-LF-WB and WENO7-LF-WB are shown in Figure 10. While no visible differ-
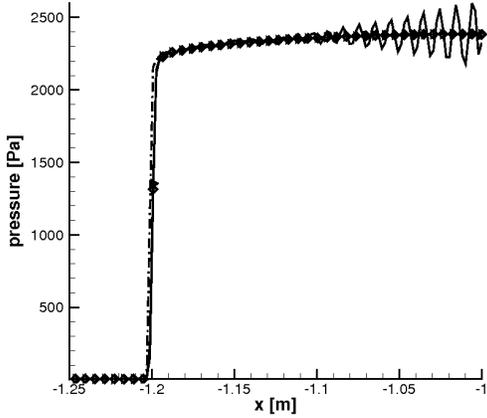
FIGURE 1. Stagnation line pressure on coarse mesh: TVD (dashdot line), WENO5-LF (right triangles), WENO7-LF (diamonds), WENO9-LF (solid line).
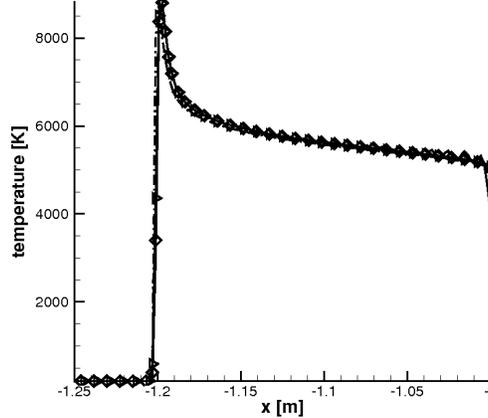

FIGURE 2. Stagnation line temperature on coarse mesh: TVD (dashdot line), WENO5-LF (right triangles), WENO7-LF (diamonds), WENO9-LF (solid line).
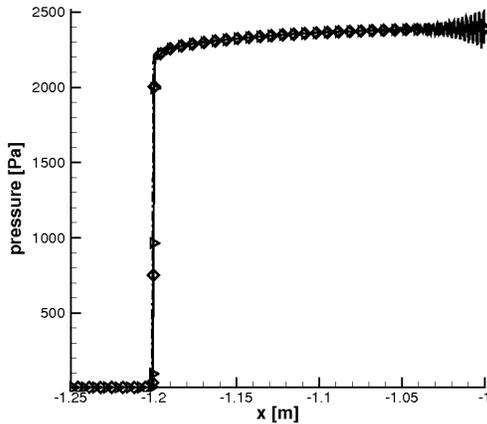

FIGURE 3. Stagnation line pressure on fine mesh: TVD (dashdot line), WENO5-LF (right triangles), WENO7-LF (diamonds), WENO9-LF (solid line).
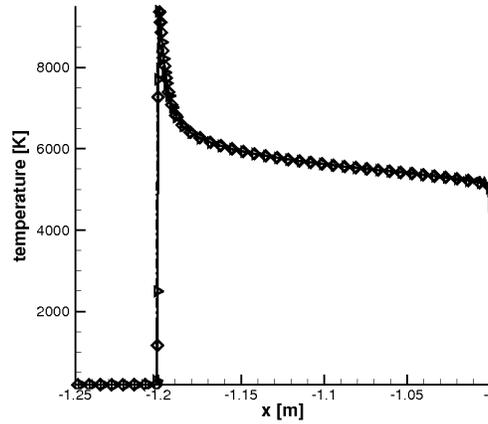

FIGURE 4. Stagnation line temperature on fine mesh: TVD (dashdot line), WENO5-LF (right triangles), WENO7-LF (diamonds), WENO9-LF (solid line).

ence appears among WENO5-LF, WENO5-LF-WB and WENO7-LF, WENO7-LF tends to predict a slightly higher temperature.

3.3. *Viscous flow: TVD on single mesh*

Gnoffo's test case has also been used to verify our implementation of diffusive terms for chemical nonequilibrium flows but only with the TVD scheme for now. In Figures 11 and 12 our solution on the same coarse mesh is compared with the TVD result in Wang's study in terms of pressure and temperature. Note that this is not a fair comparison as Gnoffo's test case was simulated in Wang's study with a two-temperature model. While Figure 11 shows pressure fields in perfect quantitative agreement, the shock standoff distance is slightly bigger for Wang's study, which is consistent with the fact that he also
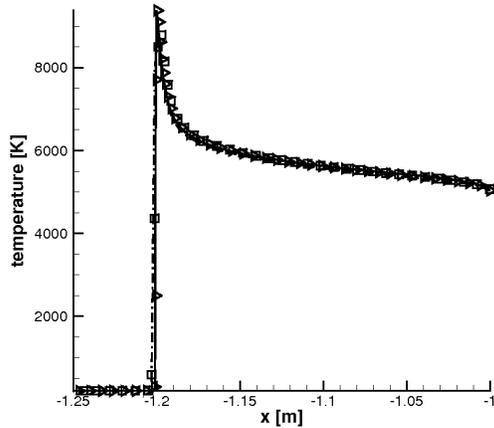
FIGURE 5. Stagnation line temperature: TVD on coarse (dashdot line) and fine mesh (solid line), WENO5-LF on coarse (squares) and fine mesh (right triangles).
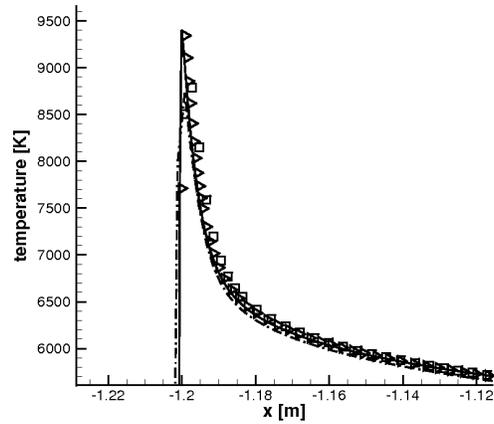

FIGURE 6. Zoom around the peak temperature: TVD on coarse (dashdot line) and fine mesh (solid line), WENO5-LF on coarse (squares) and fine mesh (right triangles).
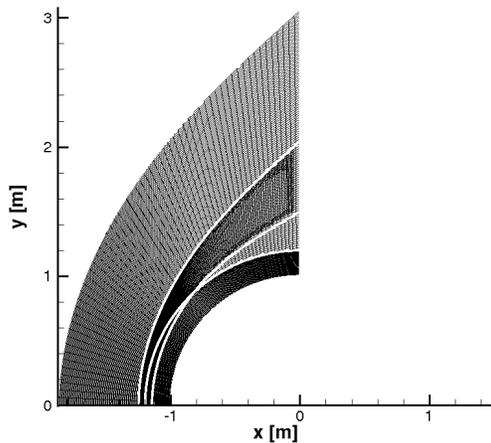

FIGURE 7. View on the upper half of the three--block overset mesh used for Gnoffo's test case. Boundaries for shock and body blocks are highlighted in white.
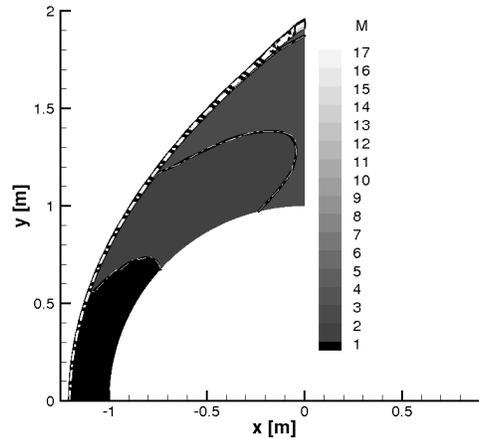

FIGURE 8. Mach number on the overset mesh: TVD (contours), WENO5-LF (black isolines), WENO7-LF (white dashdot isolines). Herein, part of the background block has been blanked.

assumed thermal nonequilibrium, leading to a higher roto-translational temperature in the post-shock region (11460 K against 8680 K), as emerges from Figure 12. A different temperature field leads to a different effective temperature for activating the chemistry, which, according to Park's model adopted by Wang's study, is a geometric average of roto-translational and vibrational temperature, whereas in our model it is the temperature itself. This fact causes discrepancies in dissociation/recombination rates. Moreover, since transport properties depend on local temperature and chemical composition of the gas mixture, and chemical composition depends on the local temperatures (one in our case, two in our reference), an impact is expected on the boundary layer properties. This effect can justify the visibly smaller boundary layer thickness in our solution.
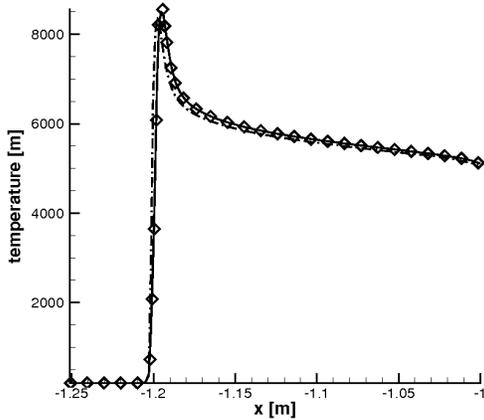
FIGURE 9. Stagnation line temperature on the three-block overset mesh: TVD (dashdot line), WENO5-LF (solid line), WENO7-LF (right triangles).
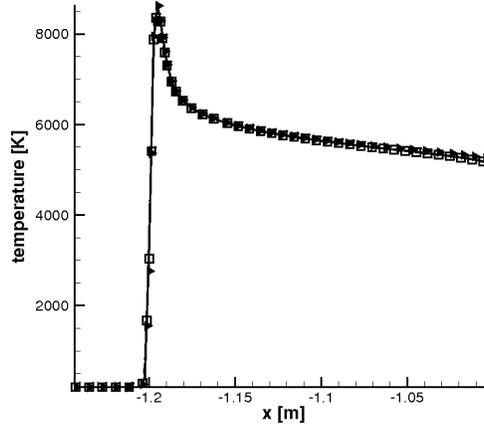
FIGURE 10. Stagnation line temperature on the overset mesh: WENO5-LF (solid line), WENO5-LF-WB(dashdot line), WENO7-LF (squares), WENO7-LF-WB (right triangles).

3.4. *Viscous flow: TVD on overset mesh*

Our implementation of nonequilibrium diffusive terms has been verified on two distinct overset meshes: the same three-block computational mesh in Figure 7 and another one sharing the same topology, but with a smaller background block and a finer resolution in both shock (3 times in normal direction) and boundary layer (6 times in normal direction). As in the previous case, all our viscous simulations have been run with the TVD scheme. In Figures 13 and 14 the solutions on single-block (fine) and three-block overset grids (both coarse and fine) are compared in terms of pressure and temperature. The pressure isolines/levels and shock standoff distance match perfectly between the fine single- and multiblock meshes. The shock refinement applied between the coarse and fine overset mesh consistently leads the solution to get closer to the fine single-block mesh case. The agreement on the temperature isolines also improves significantly while refining the overset mesh, but some differences still persist in the boundary layer region, where the single-block mesh resolution is about twice as fine as that of the overset grid.

4. Conclusions and future plans

With the present analysis, additional insight has been gained into the application of fifth- up to ninth-order WENO schemes to study nonequilibrium flows with strong bow shocks. In our numerical experiments, no significant gain has been identified in using WENO of order higher than fifth. Therefore, WENO5-LF or, alternatively, WENO5-LF-WB can be indicated as candidates (among the family of schemes here considered) for pursuing nonequilibrium flow computations, even though the resolution of WENO5 is slightly better than TVD. However, the most diffusive limiter has been used for TVD in our case. Some preliminary results to verify our implementation of nonequilibrium viscous flows on overset meshes have also been shown, but limited to a TVD discretization. Higher-order discretizations for the diffusive flux derivatives are included in ADPDIS3D and will be considered in future work. Since the use of higher-order schemes is beneficial particularly in smooth flows, an enhanced prediction of boundary layer properties, skin
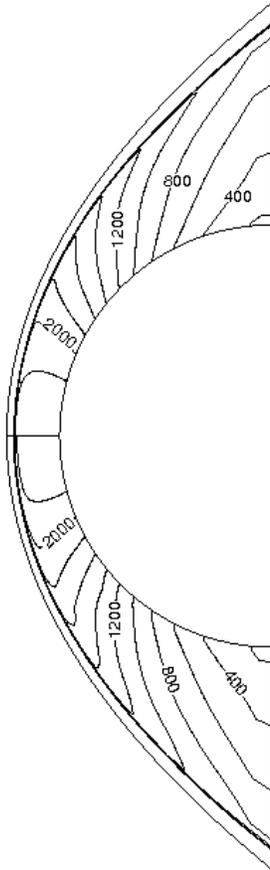
FIGURE 11. Pressure isolevels (in Pa) for Gnoffo's cylinder on coarse single-block mesh: MUTATION-based chemical nonequilibrium model (top), thermo-chemical nonequilibrium model in Wang's study (bottom).
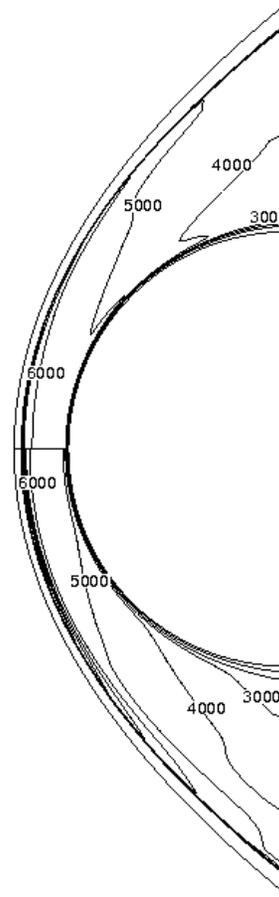
FIGURE 12. Temperature isolevels (in K) for Gnoffo's cylinder on coarse single-block mesh: MUTATION-based chemical nonequilibrium model (top), thermo-chemical nonequilibrium model in Wang's study (bottom).

friction and thermal loads on relatively coarse overset meshes is expected when applying variable high-order finite difference methods to nonequilibrium flows. Those schemes will combine WENO (or TVD) schemes close to the bow shock and sixth- or higher-order filter central discretizations elsewhere. Future efforts will focus on evaluating such possible benefits and in performing a more challenging mixed steady/unsteady 3D simulation of the high- speed chemically reactive flow around the NASA Crew Exploration Vehicle (CEV) with variable high-order filter schemes based on some of the schemes here described. A preliminary study on the full CEV configuration (nonreactive gas simulated with TVD scheme) is described in Lani *et al.* (2010). Extension of the current chemical nonequilibrium model to a multitemperature approach is envisioned in order to include thermal relaxation processes that can significantly affect the actual chemical kinetics in high-temperature gas, especially in regions (e.g., afterbody) characterized by expanding flows.
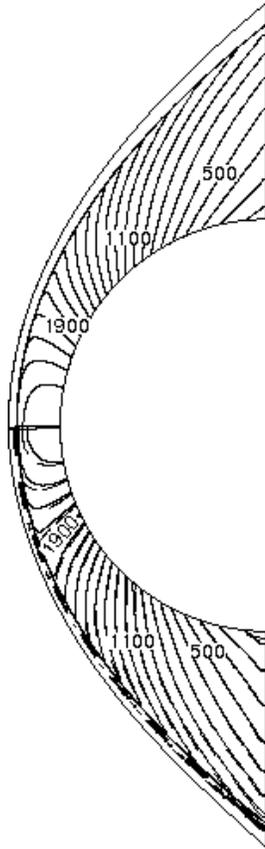
FIGURE 13. Pressure field (in Pa): isolines and levels on fine (top) single-block mesh, on coarse (bottom, dashed line) and fine (bottom: solid line) overset mesh.
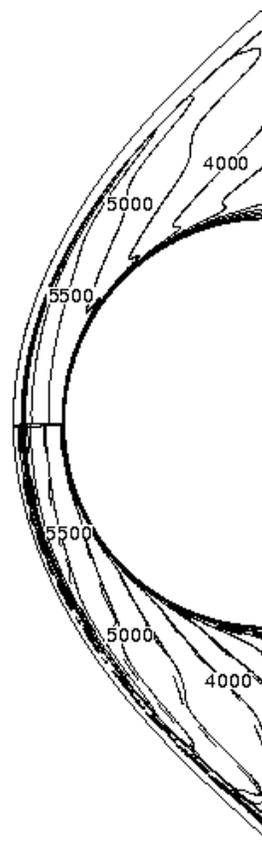
FIGURE 14. Temperature field (in K): isolines and levels on fine (top) single-block mesh, on coarse (bottom, dashed line) and fine (bottom: solid line) overset mesh.

Acknowledgments

REFERENCES

ABEELE, D. V. 2000 An efficient computational model for inductively coupled air plasma flows under thermal and chemical non-equilibrium. PhD thesis, Katholieke Universiteit Leuven, Chaussée de Waterloo, 72, 1640 Rhode-St-Genèse, Belgium.

HADJADJ, A., YEE, H. C. & SJÖGREEN, B. 2010 LES of temporally evolving mixing layers by high order filter schemes Submitted to *J. Comput. Phys.*

HARTEN, A. 1984 On a class of high resolution total variation stable finite difference schemes. *SIAM J. Num. Anal.* **2**, 1–23.

JIANG, G. S. & SHU, C. W. 1996 Efficient implementation of weighted ENO schemes. *J. Comput. Phys.* **126**, 202–228.

LANI, A., SJÖGREEN, B. & YEE, H. C. 2010 Computational study of hypersonic flow past a CEV-like capsule on multiblock overlapping grids. Annual research brief. Centre for Turbulence Research, Stanford University.

MAGIN, T. & DEGREZ, G. 2004 Transport algorithms for partially ionized and unmagnetized plasmas. *J. Comput. Phys.* **198**, 424–449.

PARK, C. 1993 Review of chemical-kinetic problems of future nasa mission, I: Earth entries. *J. Thermophys. & Heat Transfer* **7**, 385–398.

SJÖGREEN, B. & YEE, H. C. 2009 Variable high order multiblock overlapping grid methods for mixed steady and unsteady multiscale viscous flow. *Comm. in Comput. Phys.* **5** (2-4), 730–744.

SJÖGREEN, B., YEE, H. C., DJOMEHRI, J., LAZANOFF, A. & HENSHAW, W. D. 2009 Parallel performance of adpdis3d - a high order multiblock overlapping grid solver for hypersonic turbulence. Parallel CFD, Moffett Field (CA).

WANG, W., SHU, C. W., YEE, H. C. & SJÖGREEN, B. 2009 High-order well balanced schemes and applications to non-equilibrium flows. *J. Comput. Phys.* **228**, 6682–6702.

WANG, W., YEE, H. C., SJÖGREEN, B., MAGIN, T. & SHU, C. W. 2010 Construction of low dissipative high-order well balanced filter schemes for non-equilibrium flows. *J. Comput. Phys.* .

YEE, H. & SJÖGREEN, B. 2009 High order filter methods for wide range of compressible flow speeds. In *Proceedings of ICOSAHOM 09, International Conference on Spectral and High Order Methods*. Trondheim, Norway.

YEE, H. C. 1989 A class of high-resolution explicit and implicit shock-capturing methods. In *VKI lecture series 1989-04*. NASA TM-101088.

YEE, H. C. & SJÖGREEN, B. 2006 Efficient low dissipative high order schemes for multiscale mhd flows, II: Minimization of div(b) numerical error. *J. Sci. Comp.* **29**, 115–16.

YEE, H. C. & SJÖGREEN, B. 2006 Nonlinear filtering and limiting in high order methods for ideal and non-ideal mhd. *J. Sci. Comp.* **27**, 507–521.

YEE, H. C., SJÖGREEN, B. & BARONE, M. 2008 High order numerical schemes for hypersonic flow simulations. In *VKI Lecture Series: Course on hypersonic entry and cruise vehicles*. Von Karman Institute for Fluid Dynamics, Stanford University, Palo Alto (CA).

YEE, H. C., SJÖGREEN, B. & HADJADJ, A. 2010 Comparative study of high order schemes for LES of temporally evolving mixing layers Extended version of the paper for the Proceedings of ASTRONUM-2010, June 13-18, 2010, San Diego, Calif; submitted to *J. Comp. & Fluids.*